Sustainable Materials and Technologies 16 (2018) 12–22

Contents lists available at ScienceDirect

Sustainable Materials and Technologies

journal homepage: www.elsevier.com/locate/susmat

Density functional theory study on the effects of oxygen groups on band gap tuning of graphitic carbon nitrides for possible photocatalytic applications

Binghua Jing[a], Zhimin Ao[a,*], Zhenyuan Teng[b], Chengyin Wang[b], Jiabao Yi[c], Taicheng An[a]

[a] *Guangzhou Key Laboratory of Environmental Catalysis and Pollution Control, Institute of Environmental Health and Pollution Control, School of Environmental Science and Engineering, Guangdong University of Technology, Guangzhou 510006, China*

[b] *College of Chemistry and Chemical Engineering, Jiangsu Key Laboratory of Environmental Engineering and Monitoring, Yangzhou University, 180 Si-Wang-Ting Road, Yangzhou 225002, China*

[c] *School of Materials Science and Engineering, The University of New South Wales, Sydney, NSW 2052, Australia*

ARTICLE INFO

Keywords:
g-C_3N_4
Bandgap
Density functional theory
Photocatalysis

ABSTRACT

Graphitic carbon nitride (g-C_3N_4) has been considered to be a promising photocatalyst due to its photoresponse under visible light. It is known that different types of oxygen groups would be normally remained on g-C_3N_4 during synthesis, and g-C_3N_4 with oxygen groups was reported to have promising photocatalytic performance experimentally. To understand the mechanism of the enhanced photocatalytic performance of g-C_3N_4 with oxygen groups, density functional theory (DFT) calculations were carried out in this work to investigate the band structures of g-C_3N_4 with different types of oxygen groups (−COOH, −OH or =O) systematically, thus predicting its capability of activation of electron-hole pair. In addition, in order to consider the position of oxygen groups on g-C_3N_4 and its corresponding effect on the band structure, graphitic carbon nitride nanoribbons (CNNR) is built. It is found that only −OH and =O groups can be stably attached at the center of CNNR, while all the three types of groups are stable at the edges. Additionally, −COOH or −OH group binding with N atoms (N−COOH or N−OH) can reduce the bandgap of CNNR significantly, and the bandgap further reduces sharply at high concentration of N−COOH or N−OH, while attaching =O does not change its bandgap much regardless the position of the groups expect replacing H atom at the right edge. Therefore, attaching N−OH at the middle, replacing H atoms by =O at the right edge and attaching N−COOH or N−OH at both sides are promising ways to reduce the band gap of CNNR and thus may improve the generation of electron-hole pair. Furthermore, the higher the concentration of the oxygen groups, the better the performance it has.

1. Introduction

Nanostructured materials in the application of solar energy for photocatalysis have attracted significant research attention [1–4]. Over the past few decades, various photocatalytic nanomaterials, which have large surface area for providing more active sites, and enhance the interfacial electron/hole activation and separation, have shown preferable activity compared to their bulk counterparts [5,6]. Basically, they accelerate the photocatalytic process based on the enhanced capability of electron-hole pairs [7] activation or the reduction of activated electron-hole recombination of a semiconductor photocatalyst [8,9].

During the photoirradiation, once the energy is superior to the excitation energy of nanostructured photocatalysts, photoexcitation consequently leads to a spatial charge separation between the electron in the conduction band and the hole in the valence band [10]. The electron–hole pair would induce the formation of active radicals for photocatalytic decomposition of surface molecules on the photocatalysts. The design of band structure alignment of semiconductors is generally adopted to promote the activation of electrons, meanwhile to facilitate the separation of charge carriers at the interfaces of semiconductor [1,10]. Thus, one of the key factors for the photocatalytic performance is the capability for the photo-activation of electron-hole pairs [11], which is determined by the band structure of the photocatalysts, such as the band gap and positions of conductive and valance bands. In other words, a significant reduction of the band gap favours the photogeneration of electron and hole pairs [12].

Graphitic carbon nitride (g-C_3N_4), which has been recognized as polymeric metal-free photocatalysts with *sp* [2] conjugation for both green synthetic chemistry and solar energy conversion, has attracted tremendous interest in electronics and optoelectronics [10,13–20]. Nano-sized g-C_3N_4 (N-g-C_3N_4) possesses enormous advantages compared with bulk g-C_3N_4, such as the significantly larger specific surface

---

* Corresponding author.
E-mail address: zhimin.ao@gdut.edu.cn (Z. Ao).

https://doi.org/10.1016/j.susmat.2018.04.001
Received 28 February 2018; Received in revised form 29 March 2018; Accepted 2 April 2018

area with abundant active sites [21–24]. g-C_3N_4 is a low cost photocatalyst, and shows high stability under both acidic and alkaline conditions [12]. As an effective and all-organic photocatalyst, a variety of photocatalytic performance has been realized. Huang et al. first found that g-C_3N_4 was an effective, recyclable catalyst for bacterial inactivation in water under visible light irradiation, without any *E. coli* K-12 bacterial regrowth [7]. Zhao et al. first reported the fabrication of the single layer g-C_3N_4 could be applied in photocatalytic disinfection due to the efficient photo-generated charge separation under visible light irradiation [25]. In addition, Wang et al. observed efficient hydrogen production for the first time from visible-light photocatalysis on g-C_3N_4 [10,26]. However, the relatively large band gap 3.02 eV [12] of pristine g-C_3N_4 limits its visible-light absorption.

Currently, oxidization exfoliation and etching are common strategies for N-g-C_3N_4 preparation with advantages of low cost and easy operation [15,22,27]. g-C_3N_4 can be partly oxidized at these drastic oxidization conditions [22,24,28] and different types of oxygen groups may be introduced into N-g-C_3N_4 during synthesis process [22,28,29]. Functional groups may enable the manipulation of various properties [30]. Compared with pristine g-C_3N_4, N-g-C_3N_4 based photocatalysts functionalized by oxygen groups (N-O_x-g-C_3N_4) have shown their significantly enhanced photocatalytic performance. For example, She et al. found N-O_x-g-C_3N_4 showed outstanding photocatalytic performance for hydrogen production from water and degradation of the organic pollutant under visible light irradiation [31,32]. Simultaneously, Huang et al. reported that the material exhibited significantly enhanced solar-energy-driven hydrogen evolution reaction activity compared with bulk g-C_3N_4 and supra-molecular-induced 3D porous g-C_3N_4 [33]. The enhanced photocatalytic performances of N-O_x-g-C_3N_4 were mostly explained by the increased photo carriers, which can be attributed to the enhanced quantum confinement effects [24,25] and the unbalanced charge distributions caused by the attached oxygen groups [28,31,32]. However, the exact mechanism is not very clear. Therefore, in order to provide theoretical guidance for the design and synthesis of specific carbon nitrides for potential photocatalytic applications, influences of different types of oxygen functional groups on the band structure of N-g-C_3N_4 should be investigated in details.

In this work, theoretical models of graphitic carbon nitride nanoribbons (CNNR) were built to investigate the effects of three typical types of oxygen groups ($-$COOH, $-$OH and $=$O) [34] on CNNR and their influences on the band structures based on density functional theory (DFT) calculations. All possible binding positions of $-$COOH, $-$OH and $=$O groups on CNNR were considered and analyzed to determine the favourite configurations. After the optimization of the atomic structures, the corresponding band structures are also calculated and the mechanisms of bandgap engineering of the g-C_3N_4 are discussed.

2. Calculation methods

The DFT calculations in this work were implemented in DMOL3 modulus [35,36]. The exchange-correlation interactions were described by generalized gradient approximation (GGA) with the Perdew-Burke-Ernzerhof (PBE) functional [37,38]. Spin-polarization was included in all calculations and a damped van der Waals correction was incorporated using Grimme's scheme to describe the non-bonding interactions [39]. The vacuum space above the g-C_3N_4 layer is 20 Å, which is considered to be big enough to eliminate the interaction between the layers in different supercells [40,41]. 0.005 Ha smearing was used in the calculations. The Brillouin zone was sampled with the Monkhorst-Pack mesh with K-points of 6 × 6 × 1 grid in reciprocal space during electronic structure calculations. The BLYP function was employed to obtain more accurate vacuum potential levels [12].

Fig. 1(a) presents the fully optimized structure for bulk g-C_3N_4. In order to investigate the edge effects of N-g-C_3N_4, the supercell [42] of g-C_3N_4 nanoribbon (CNNR) is built, as shown in Fig. 1(b). There are 20 Å vacuums besides the edges of the nanoribbon and above the nanoribbon to minimize the interaction between different nanoribbons in different supercells. To further investigate the positions of oxygen groups and the corresponding effects on the band structures of CNNR, $-$COOH, $-$OH, or $=$O oxygen group was respectively attached on the different sites of the nanoribbon: left and right edges, as well as the center of the ribbon, as indicated by the numbers in Fig. 1(b).

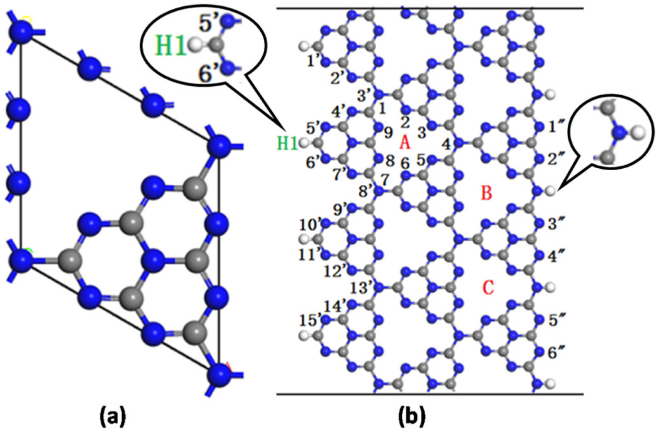

Fig. 1. The optimized structures of bulk g-C_3N_4 (a) and CNNR (b). Atom color code: carbon (grey), nitrogen (blue). The numbers in the panel (b) indicate different attaching sites for oxygen groups at the center and both sides of the nanoribbon. The letters A–C denote different holes in CNNR. To better show the edge structure, the magnified structures are inserted. (For interpretation of the references to color in this figure legend, the reader is referred to the web version of this article.)

3. Results and discussion

Based on literature reports, the contributions of external groups on changing the properties and band gap of g-C_3N_4 have been proved, *i.e.* the electrochemical response of EDTA-g-C_3N_4 nanosheets for Pb (II) detection was much more significant than of g-C_3N_4 nanosheets without EDTA [19]. Oxygen groups have demonstrated the capability to adjusting the band gap of g-C_3N_4 and significantly increase the lifetime of the photo carriers [28]. However, the influences of functionalization positions and tendency of band gap change were rarely discussed. As shown in Fig. 1(b), the model of a CNNR was built to precisely investigate effects of oxygen functionalization at different positions (the oxygen groups may attach to carbon or nitrogen. Therefore, all the possible functionalization types were considered at the two types of atoms at different positions of the CNNR as follows: N$-$COOH, C$-$⊕ COOH, N$-$OH, C$-$OH, and N$=$O, C$=$O).

After geometry optimization, the atomic structures of bulk g-C_3N_4 and CNNR are shown in Fig. 1, their corresponding band structures are present in Fig. 2(a) and (b), respectively. It is well known that band gap of a semiconductor is the energy difference between the bottom of conduction band and the top of valence band. From Fig. 2(a), it shows that the band gap of bulk g-C_3N_4 is 1.54 eV, which is smaller than the reported calculated value 1.89 eV [12], owing to the neglected self-interaction in the PBE functional used in this work, and thus underestimating the band gap, while the CNNR has a band gap of 1.25 eV as shown in Fig. 2(b). To calculate the band gap more accurately, HSE06 functional was also adopted to calculate the band structure of bulk g-C_3N_4, and the band structure is shown in Fig. S1. It is shown that the band gap is 3.03 eV, consistent with the experimental value 3.02 eV [10,12]. However, the calculation using hybrid functional is very time consuming, which is unaffordable for the calculation of a large CNNR system. In addition, we more concern on the band structure change trend of CNNRs with different type of oxygen groups, but not focus on the exact value of the band gaps. Therefore, BLYP functional was used

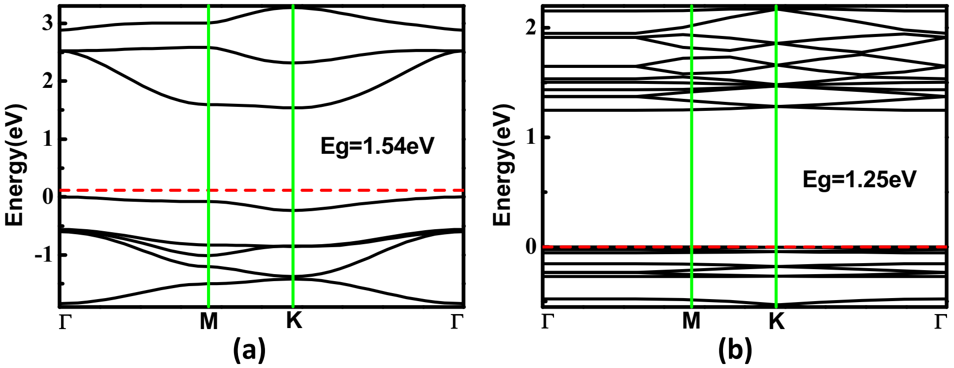

Fig. 2. The band structures of bulk g-C_3N_4 (a) and CNNR (b). The Fermi level is denoted by the red dashed line. The corresponding band gap is indicated in the figure. (For interpretation of the references to color in this figure legend, the reader is referred to the web version of this article.)

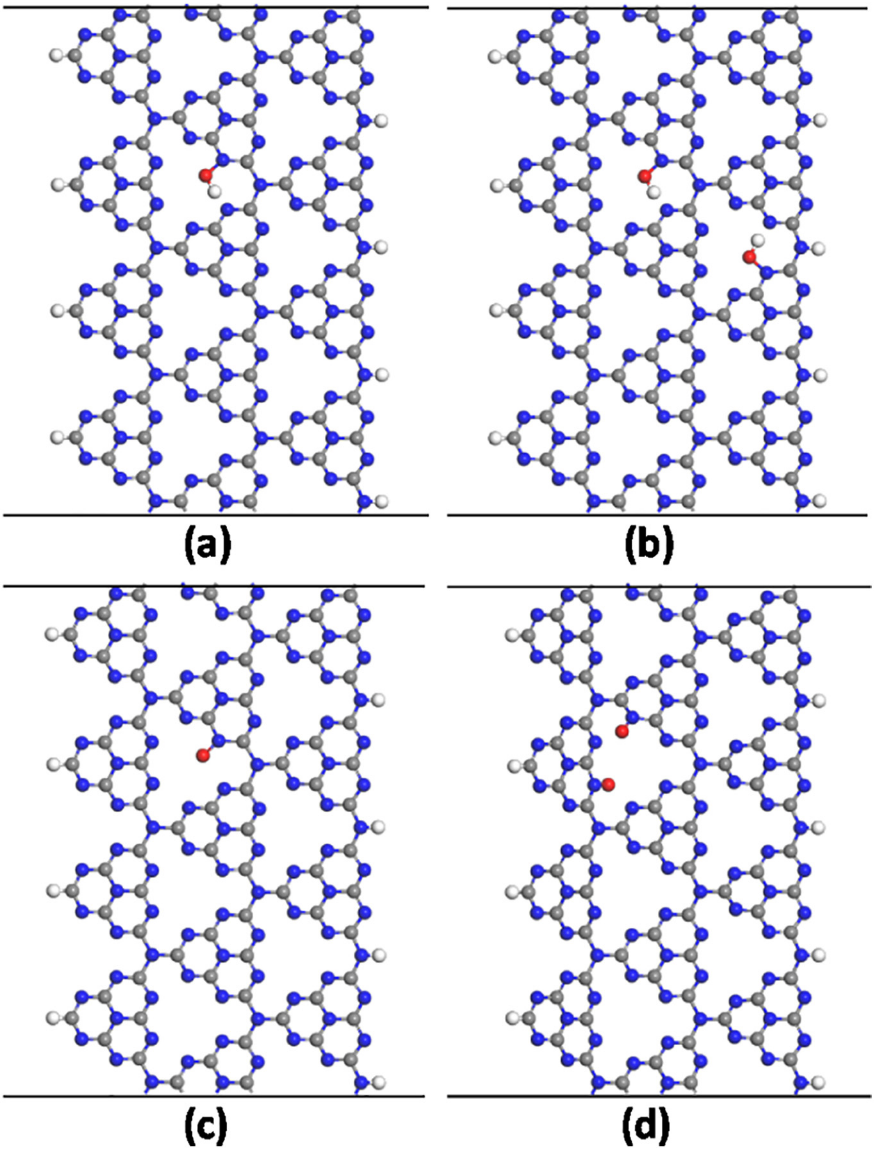

Fig. 3. The most stable structures with one −OH (a), two −OH (b), one =O (c), and two =O (d) attached at the center of CNNR.

in the following band structure calculation, and the band gap changes are discussed. As shown in Fig. 2(b), the presence of edges would reduce the band gap of g-C_3N_4, which would improve the generation of electron-hole pair under visible light irradiation significantly.

To understand the effects of oxygen functional groups on the generation of electron-hole pair under visible light irradiation, different type of oxygen groups attached at different positions are calculated as follows and their corresponding band structures are also discussed.

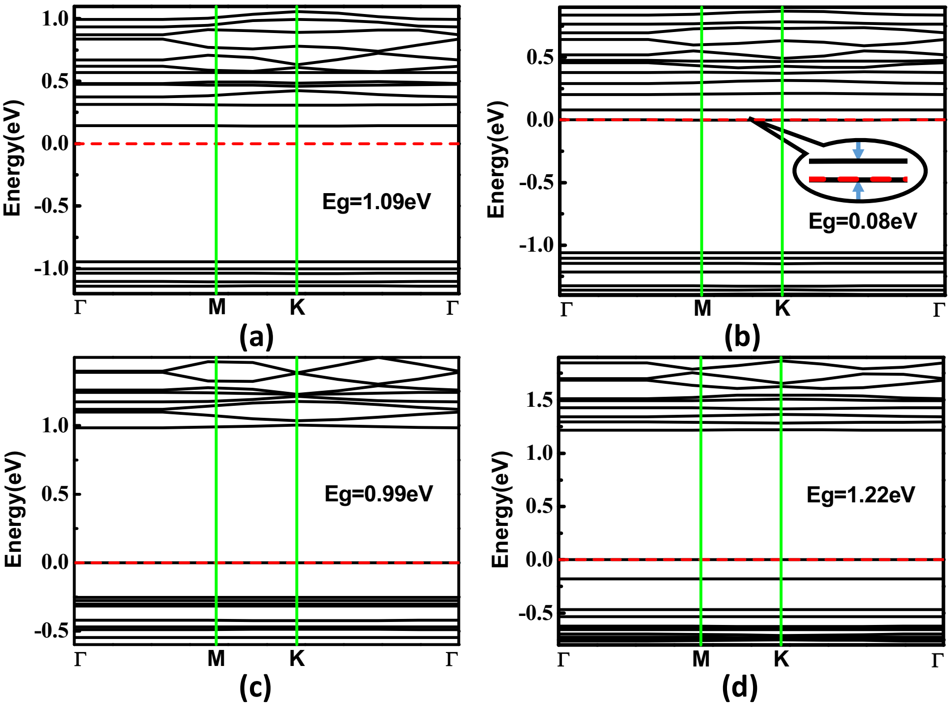

Fig. 4. The band structure of the CNNR attached one −OH (a), two −OH (b), one =O (c), and two =O (d) at the center.

3.1. Oxygen groups functionalized at the center of CNNR

Typical oxygen groups, including −COOH, −OH and =O, attached at the center of the CNNR were firstly investigated. As shown in Fig. 1(b), N atoms at positions 2, 3, 5, 6, 8 and 9 near a hole in the center of the nanoribbon bind with two C atoms, while other N atoms, such as at positions 1, 4 and 7, bind with three C atoms, *i.e.* these N atoms near the hole are more active due to the unsaturated bonds. In this way, −COOH, −OH and =O have higher possibility to attach to the N atoms at positions 2, 3, 5, 6, 8 and 9.

All possible positions for oxygen group, including C atom positions, were considered and geometry was optimized. It is found that the −COOH group is dissociated and forms =O bond with the N atoms, while −OH and =O can exist stably at the N atoms near the holes. Therefore, one −OH or =O group attached on the N atom at sites 1–9 in Area A of Fig. 1(b) is calculated respectively.

After geometry optimization, it is found that both −OH and =O prefer to attach on the N atom at Site 3, where the two configurations have the lowest total energies respectively for the two oxygen groups attachment, and the corresponding structures are shown in Fig. 3(a) and (c). To understand the effect of the concentration of oxygen group, two −OH or =O groups are attached in the center of CNNR with the second −OH or =O group attached on an N atom in the Areas A–C (Fig. 1(b)). After structure relaxation, the favourite configurations for two −OH or =O groups attached at the center of CNNR are shown in Fig. 3(b) and (d). In order to understand the effect of oxygen groups on the generation of electron-hole pair, the corresponding band structures for the configurations in Fig. 3 are shown in Fig. 4, respectively.

As shown in Fig. 4, it is obvious that, at low concentration of the oxygen groups, the band gap width of CNNR with attaching one −OH or =O decreases from 1.25 eV to 1.09 eV or 0.99 eV, respectively. If increasing the concentration of the oxygen groups, *i.e.* attaching two −OH or =O on the CNNR, the band gap decreases sharply to 0.08 eV for the case of CNNR with two −OH groups, while the band gap increases a little to 1.22 eV for the case of CNNR with two =O atoms. Through comparing the band structures in Figs. 2(b), 4(a) and (b), new band appears slight above the Fermi level, which is the new top of the valence band and should be caused by the attached −OH groups. In addition, the Fermi level together with the new top of valence band shift to the conduction band and reaches near to the bottom of the conduction band at higher concentration of −OH group, which would reduce the band gap width sharply. This phenomenon indicates that g-C_3N_4 with higher oxygen groups concentration may have the better generation of electron-hole pair.

When the concentration of =O increases, as comparing the band structures in Figs. 2(b), 4(c) and (d), the Fermi level and valence band do not shift obviously, the conductive band shifts down and up slightly after one =O and two =O attaching, and the new band slightly below the Fermi level is caused by =O. Therefore, the functional groups including N−OH and N=O attached in the center of the nanoribbon may result in narrower band gap width, and additional N−OH in the center of CNNR will significantly reduce the bandgap width of CNNR. This also demonstrates that the generation of electron-hole pair of g-C_3N_4 with −OH is superior to that with =O.

3.2. Oxygen groups functionalized at the left edge of CNNR

To further investigate the effect of the positions of oxygen groups and tendency of bandgap change at CNNR edges, the stability of CNNR functionalized by oxygen groups (−COOH, −OH and =O) at both edges, including big zigzag edge (left side) and small zigzag edge (right side), is investigated, and the model for the calculation is shown in Fig. 1(b). As mentioned above, oxygen groups may prefer to attach to N atoms (these functionalized groups are simply as N−COOH, N−OH and N=O), the influences of these oxygen groups at the left edge of CNNR were then investigated. Fifteen possible attaching sites for a single oxygen group at the left edge were indicated as 1′–15′, which is shown in Fig. 1(b).

After structure relaxation, the most stable configurations of CNNR with N−COOH, N−OH and N=O attached at its left side are shown in Figs. 5(a), 5(c) and 5(e), respectively. If further increasing the concentration of the oxygen groups, *i.e.* two N−COOH or N−OH or N=O attached on the left edge, the most stable structures were also calculated and shown in Fig. 5(b), (d) and (f), respectively. These optimization results indicate the stability configuration of N−COOH or N−OH or N=O at the left edge.

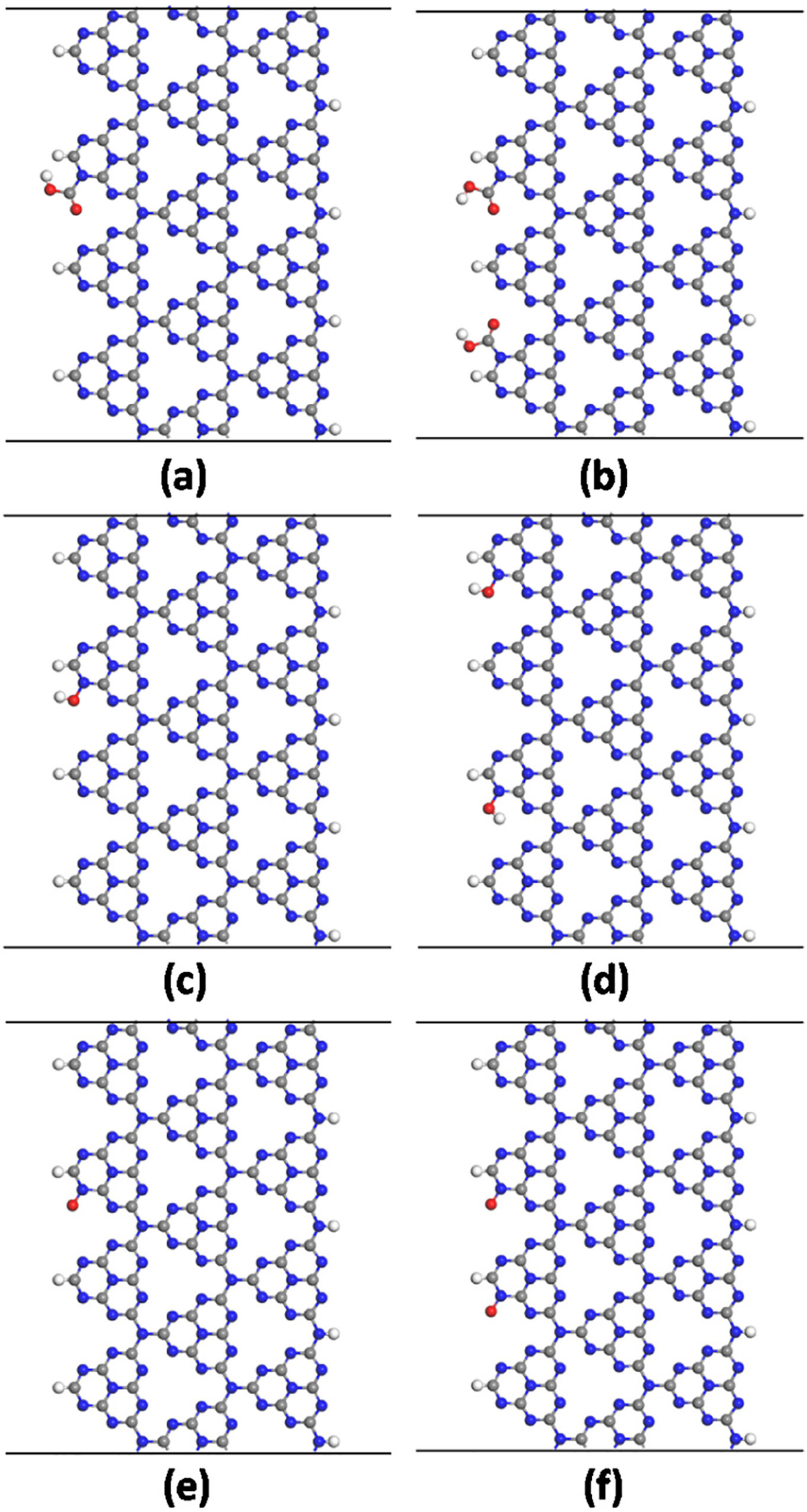

Fig. 5. The most stable configurations of CNNR with one −COOH (a), two −COOH (b), one −OH (c), two −OH (d), one =O (e) and two =O (f) attached at the left side of the nanoribbon.

After the structure optimization, the corresponding band structures of CNNR with different oxygen groups at left edge and different concentrations are showed in Fig. 6. When single N−COOH or N−OH or N=O is attached respectively at the left edge of CNNR, the band gap of these functionalized CNNR decreases obviously. The band gap of CNNR is reduced to 0.39 eV with −COOH attached, 0.34 eV with −OH

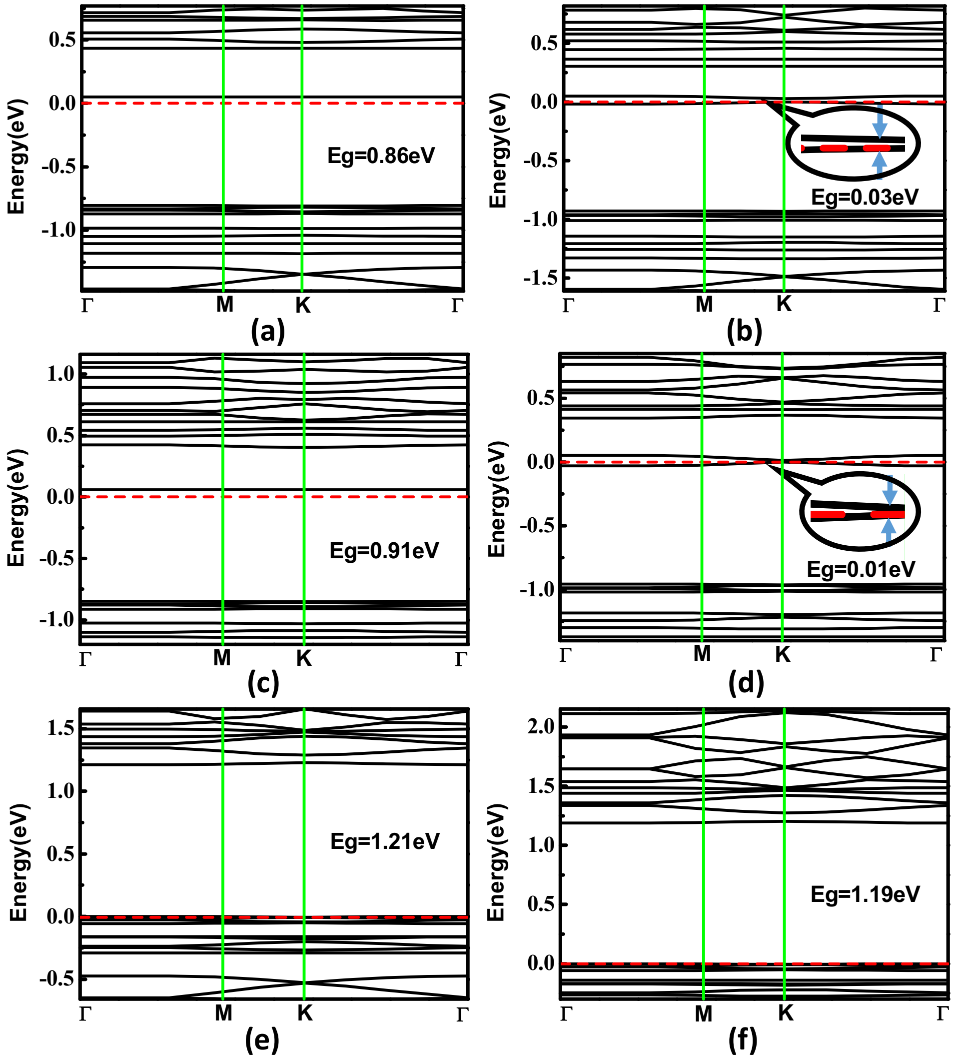

Fig. 6. The band structures of CNNR attached one $-COOH$ (a), two $-COOH$ (b), one $-OH$ (c), two $-OH$ (d), one $=O$ (e) and two $=O$ (f) at the left side of the nanoribbon.

attached and 0.04 eV with $=O$ attached, and the corresponding band structures are shown in Fig. 6(a), (c) and (e), respectively. Therefore, the oxygen group of $N-COOH$ on the left edge shows the best performance for reducing the band gap of the CNNR. Similar to the cases of attaching at the center of the CNNR, the oxygen groups are able to cause new band near the Fermi level. The new band is between the conduction band and valence band, but more close to the conduction band for the cases of attaching $-COOH$ and $-OH$, while the new band and the Fermi level are almost next to the valance band for the case of attaching $=O$. Therefore, as shown in Fig. 6(a) and (c), the appearance of the new band can significantly reduce the bandgap in the cases of functionalization by $N-COOH$ and $N-OH$. However, when single $N=O$ is functionalized at the left edge of CNNR, the new band is much close to the valance band. Hence the bandgap between conduction and valance band only shows a slight reduction. In other words, attaching $N-OH$ and $N-COOH$ groups at the left edge of CNNR may be able to achieve a better performance of the generation of electron-hole pair.

Influences of oxygen groups at different concentration levels on the band structure of the CNNR are also evaluated. When two $-COOH$ or $-OH$ or $=O$ are attached on the left edge of CNNR, the band gap width reduces sharply to 0.03 eV ($-COOH$) and 0.01 eV ($-OH$), respectively. Compared with the band structure of the CNNR functionalized by single oxygen group, it can be seen that one more band appears near the Fermi level when these groups are attached. The Fermi level of the functionalized CNNRs also shifts upward slightly and locates between the two bands caused by the two $-COOH$ or $-OH$ groups. Due to the two bands close to each other, the corresponding bandgap reduces sharply. However, when two $=O$ were attached on the left of CNNR, the bandgap does not change obviously. As shown in Fig. 6(f), the two bands caused by the two $=O$ below the Fermi level are closed to the valance band. Therefore, attaching $-COOH$ or $-OH$ at the left edge of the CNNR is also a promising way to reduce the band gap of g-C_3N_4 and improve the performance of the generation of electron-hole pair, the higher the concentration, the better the performance it would have. However, the attachment of $=O$ does not affect much on the generation of electron-hole pair.

In addition, it is also possible that the oxygen groups may replace the H atoms (the H1 site in Fig. 1(b)). After relaxation, it is found that the $-COOH$ group is not stable at H1 sites. The most stable configurations with $-OH$ and $=O$ attaching are shown in Fig. 7(a) and (c), respectively. The corresponding band structures are shown in Fig. 7(b) and (d), where the band gap for the cases of $-OH$ and $=O$ are 1.27 eV and 1.26 eV, respectively, which are slightly higher than the band gap 1.25 eV of CNNR without oxygen-containing groups. The influence of $C-OH$ and $C=O$ on the bandgap are consisted with the experimental result [28], *i.e.* the existence of $C-OH$ and $C=O$ at the edge of CNNR could be able to increase the band bap width of g-C_3N_4.

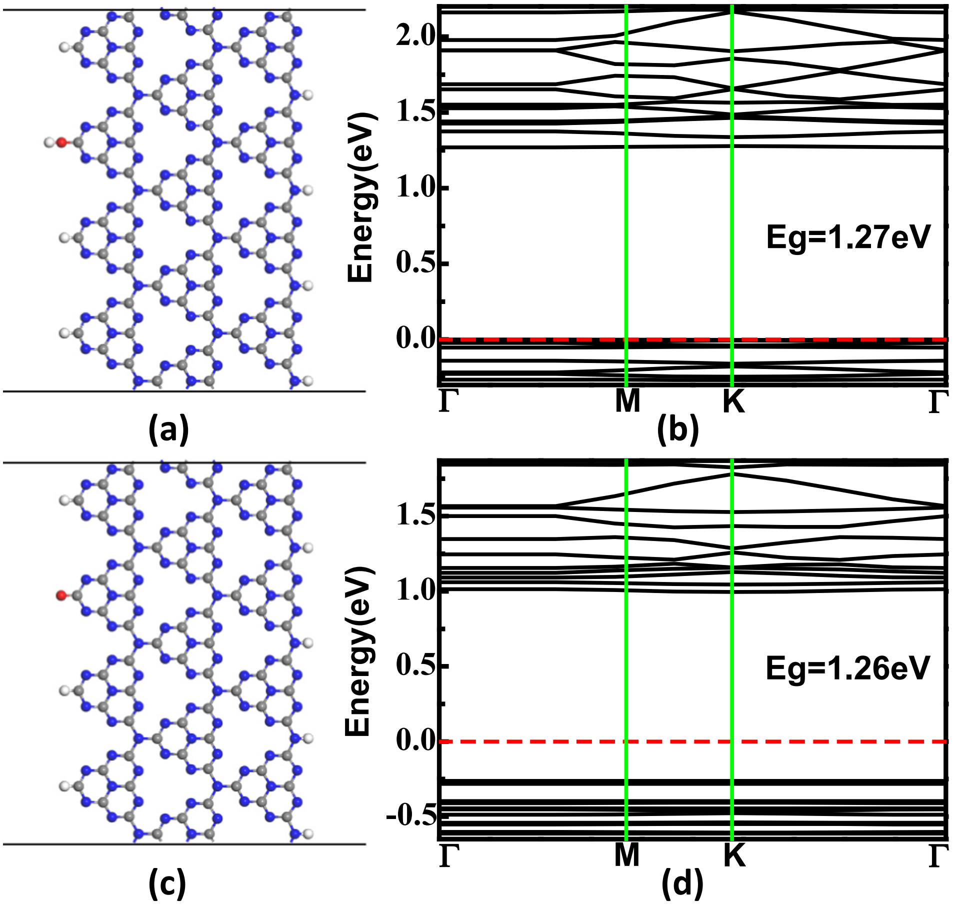

Fig. 7. The most stable atomic structure of CNNR with —OH at H1 site (a) and the corresponding band structure (b), the most stable atomic structure of CNNR with =O at H1 site (c) and the corresponding band structure (d).

3.3. Oxygen groups functionalized at the right edge of CNNR

Possible sites for single oxygen groups (—COOH or —OH or =O attached to the N atoms) at the right edge of CNNR were further investigated. All the possible sites considered are marked as 1″–6″ in Fig. 1(b), and it is found that the three oxygen-containing groups all prefer to attach at site 3″, and their most stable configurations are displayed in Fig. 8(a), (c) and (e), respectively. The concentration effect of the oxygen groups on the right edge is also considered, and the favourite configurations of the CNNR with two —COOH or —OH or =O at the right edge are displayed in Fig. 8(b), (d) and (f), respectively.

The corresponding band structures are shown in Fig. 9(a–f). Similar to the case of attaching oxygen groups at the left edge, attaching any one of the oxygen groups (—COOH or —OH or =O) at the right edge can also reduce the band gap. The band gap is reduced to 0.23 eV for the case of —COOH, 0.17 eV for the case of —OH and 0.10 eV for the case of =O. If further increasing the concentration of oxygen groups, *i.e.* two —COOH or —OH or =O attach on the right edge, the band gap reduces sharply to 0.11 eV and 0.06 eV for the cases of —COOH and —OH, respectively. On the contrast, the band gap increases a little from 1.15 to 1.16 eV for the case of =O if doubling the concentration of the oxygen group. The changing mechanism of bandgap is also similar to the case of the left edge, *i.e.* the presence of —COOH and —OH can induce new band near the Fermi level, which also locates in between the conduction and valence band, thus reducing the bandgap. If two —COOH or —OH attached, two new bands appear, and the Fermi level is located between the two bands. The band gap thus reduced sharply. For the case of =O, both of the new bands are close to the valance band, and the Fermi level is at the top of the new bands, which result in only slight change of the band gap.

In addition, at the right edge, the situation of oxygen groups replacing H atoms (the H site at the right edge in Fig. 1(b)) is also considered. After structure optimization, all of the replacement of the three oxygen groups at the site of the H atom showed acceptable stability, and the most stable structure is shown in Fig. S2. The changed band gaps (Fig. S3) for the cases of —COOH and —OH are all 1.25 eV, which is consistent with the bandgap of CNNR without oxygen groups. The most stable configurations with =O attaching are shown in Fig. 10(a) and (c), respectively. The corresponding band structures are shown in Fig. 10(b) and (d), where the bandgap for the cases with one and two =O are 0.72 eV and 0.10 eV, respectively, which are much lower than the band gap 1.25 eV of CNNR without oxygen-containing groups. Increasing the concentration of =O, would narrow the bandgap width sharply. In other words, the functionalization of =O, which replaces H atoms at the right edge, can also reduce the bandgap and improve the generation of electron-hole pair. Therefore, attaching —COOH or —OH and =O replacing H atoms at the right edge of CNNR can reduce the band gap obviously, and increasing the concentration would narrow the band gap sharply. In other words, =O replacing H atoms and attaching N—COOH and N—OH on the right edge of CNNR can be able to improve

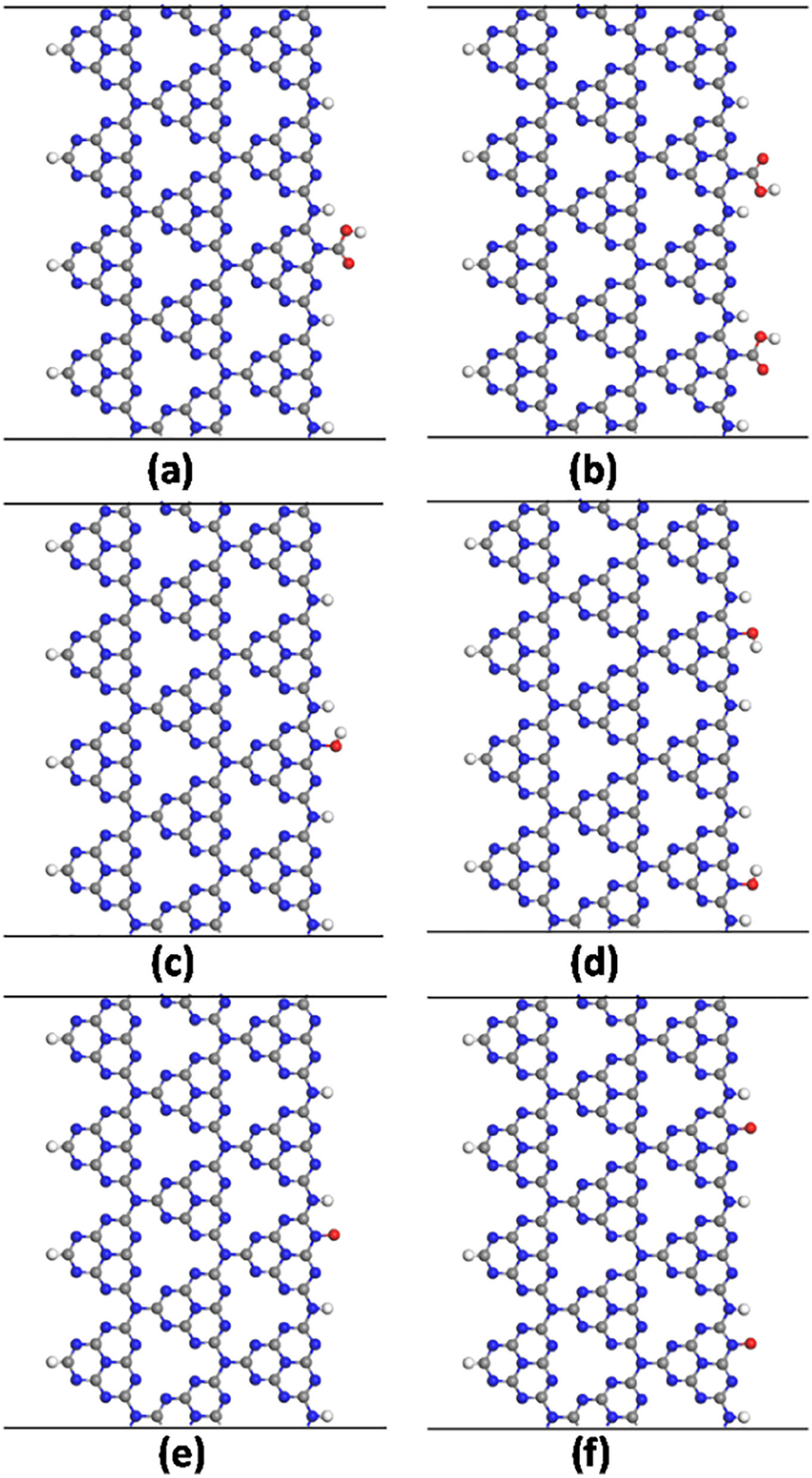

Fig. 8. The most stable structures of CNNR with one $-COOH$ (a), two $-COOH$ (b), one $-OH$ (c), two $-OH$ (d), one $=O$ (e) and two $=O$ (f) attaching at the right side of the nanoribbon.

the performance of the generation of electron-hole pair significantly.

However, computational calculations in this work are at ideal conditions with vacuum environment, while g-C_3N_4 is purely monolayer. In experiment, g-C_3N_4 may have few layers or multilayers, and in solution or gas environment. If considering the environment or layer thickness effect, the results may be different. Due to complexity of

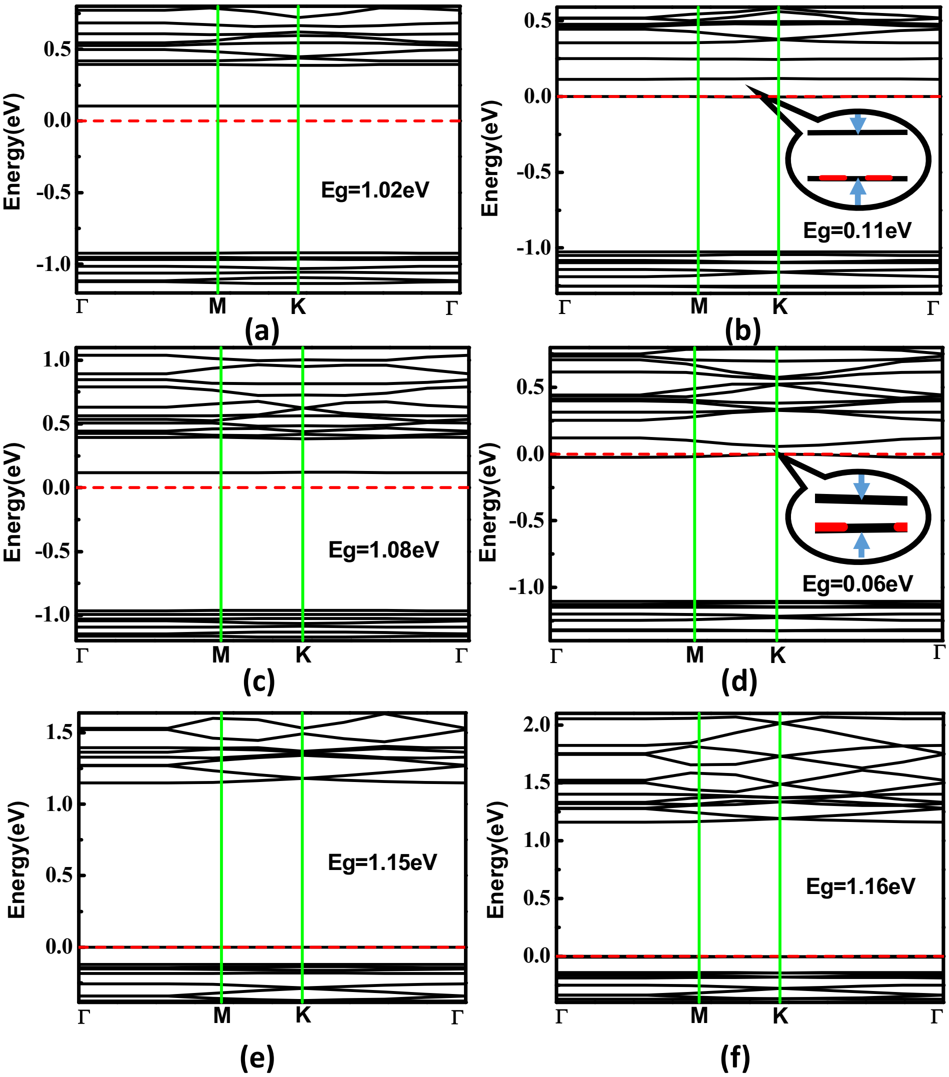

Fig. 9. The band structure of CNNR attaching one −COOH (a), one −OH (c), one =O (e), two −COOH (b), two −OH (d) and two =O (f) at the right side of the nanoribbon.

these factors, their effects will be discussed in our following works. In this study, the aim is to understand the mechanisms of high photocatalytic performance of nanostructured g-C_3N_4 based on the tuning of band gap, providing fundamental references to design of carbon nitride based semiconductors with tunable band structure to achieve the ideal generation of electron-hole pair. On the other hand, the reduction of the band gap may also facilitate the recombination of the excited electron-hole pair. Previous studies report that the reduction of band gap of g-C_3N_4 can improve the photocatalytic performance remarkably based on the both theoretical and experimental studies [12,33]. In other words, effect of the enhanced electron-hole pair generation should be more notable than that of their recombination.

4. Conclusions

In conclusion, DFT calculations were used to study the band structure of oxygen groups functionalized g-C_3N_4. Different groups, including −COOH, −OH and =O, different concentrations of the attached oxygen groups, and a variety of attaching positions, such as edges and center of g-C_3N_4 of nanoribbons, were considered. In this study, the effects of oxygen groups on g-C_3N_4 of photocatalytic performance can be understood. It is found that only N−OH and N=O can be stably attached at the center of CNNR, and all the three types of groups are stable at the edges. N−COOH or N−OH can significantly reduce the band gap of CNNR and the bandgap would narrow sharply at high concentration of these oxygen groups, regardless the position of the attached oxygen groups. However, attaching =O alone does not change the band gap much, unless replacing H atoms at the right edge. The presence of −COOH and −OH can induce new band near the Fermi level and the new band locates between the conduction and valence bands, thus reducing the band gap remarkably. Therefore, the functioned oxygen groups can tune the band structure of *g*-C_3N_4, thus tuning the generation of electron-hole pair of g-C_3N_4. Through this work, the mechanisms of higher performance of nanostructured g-C_3N_4 can be understood and it provides fundamental guidance to improve its performance for the potential photocatalytic applications.

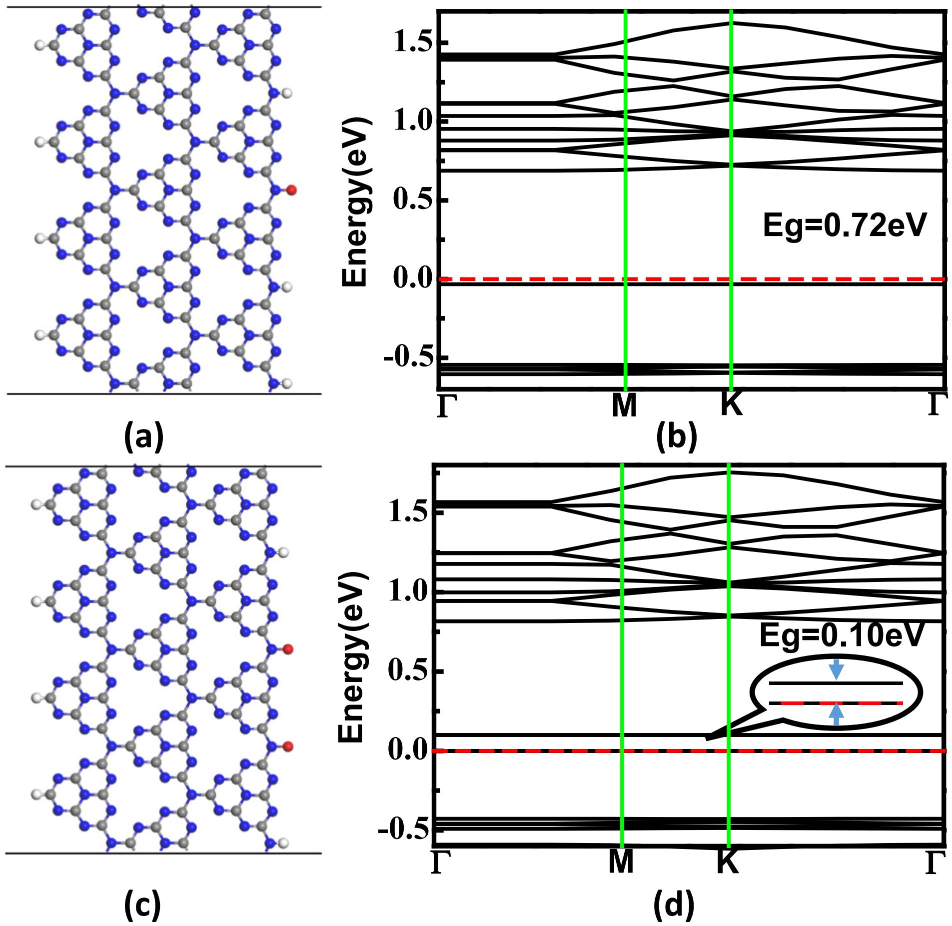

Fig. 10. The most stable structures of CNNR with one =O (a), two =O (c) at H atom site, and the corresponding band structures of CNNR with one =O (b), and two =O (d) at H atom site on the right side of the nanoribbon.

Acknowledgements

This work was supported by the National Natural Science Foundation of China (21607029, 21777033, 21375116), Science and Technology Program of Guangdong Province (2017B020216003), Science and Technology Program of Guangzhou City (201707010359), “1000 plan” for young professionals program of China, “100 talents” program of Guangdong University of Technology, the National Supercomputing Centre in Guangzhou (NSCC-GZ), the Priority Academic Program Development of Jiangsu Higher Education Institutions, Jiangsu Province research program on analytical methods and techniques on the shared platform of large-scale instruments and equipment (BZ 201409) and Project for College Graduates Jiangsu Province (KYLX16_1384).

Appendix A. Supplementary data

The band structure of bulk g-C_3N_4 using the HSE06 hybrid functional.

The most stable configurations and band structure of −COOH and −OH replacing H atoms at the right edge. Supplementary data to this article can be found online at doi:https://doi.org/10.1016/j.susmat.2018.04.001.

References

[1] J.C. Yu W Wang, D. Xia, P.K. Wong, Y. Li, Graphene and g-C_3N_4 nanosheets cowrapped elemental alpha-sulfur as a novel metal-free heterojunction photocatalyst for bacterial inactivation under visible-light, Environ. Sci. Technol. 47 (2013) 8724–8732.

[2] R. Asahi, T. Morikawa, T. Ohwaki, K. Aoki, Y. Taga, Visiblelight photocatalysis in nitrogen-doped titanium oxides, Science 293 (2001) 269–271.

[3] H.G. Kim, D.W. Hwang, J.S. Lee, An undoped, single-phase oxide photocatalyst working under visible light, J. Am. Chem. Soc. 126 (2004) 8912–8913.

[4] J.C. Yu, J. Yu W Ho, H. Yip, P.K. Wong, J. Zhao, Efficient visible-light-induced photocatalytic disinfection on sulfurdoped nanocrystalline titania, Environ. Sci. Technol. 39 (2005) 1175–1179.

[5] W. Wang, G. Li, D. Xia, T. An, H. Zhao, P.K. Wong, Photocatalytic nanomaterials for solar-driven bacterial inactivation: recent progress and challenges, Environ. Sci. Nano 4 (2017) 782–799.

[6] T. Liao, C. Sun, Z. Sun, A. Du, S. Smith, Chemically modified ribbon edge stimulated H_2 dissociation: a first-principles computational study, Phys. Chem. Chem. Phys. 15 (2013) 8054–8057.

[7] J. Huang, W. Ho, X. Wang, Metal-free disinfection effects induced by graphitic carbon nitride polymers under visible light illumination, Chem. Commun. (Camb.) 50 (2014) 4338–4340.

[8] F. Vatansever, W.C. de Melo, P. Avci, D. Vecchio, M. Sadasivam, A. Gupta, R. Chandran, M. Karimi, N.A. Parizotto, R. Yin, G.P. Tegos, M.R. Hamblin, Antimicrobial strategies centered around reactive oxygen species—bactericidal antibiotics, photodynamic therapy, and beyond, FEMS Microbiol. Rev. 37 (2013) 955–989.

[9] G. Liu, P. Niu, C. Sun, S.C. Smith, G.Q.M. Lu Z Chen, H.-M. Cheng, Unique electronic structure induced high photoreactivity of sulfur-doped graphitic C_3N_4, J. Am. Chem. Soc. 132 (2010) 11642–11648.

[10] X. Wang, K. Maeda, A. Thomas, K. Takanabe, G. Xin, J.M. Carlsson, K. Domen, M. Antonietti, A metal-free polymeric photocatalyst for hydrogen production from water under visible light, Nat. Mater. 8 (2009) 76–80.

[11] T. Liao, Z. Sun, S.X. Dou, Theoretically manipulating quantum dots on two-dimensional TiO_2 monolayer for effective visible light absorption, ACS Appl. Mater. Interfaces 9 (2017) 8255–8262.

[12] G. Gao, Y. Jiao, F. Ma, Y. Jiao, E. Waclawik, A. Du, Carbon nanodot decorated graphitic carbon nitride: new insights into the enhanced photocatalytic water splitting from ab initio studies, Phys. Chem. Chem. Phys. 17 (2015) 31140–31144.

[13] S. Naveenraj, G.J. Lee, J.J. Wu S Anandan, Nanosized tantala based materials–synthesis and applications, Mater. Res. Bull. 67((2015) 20–46.

[14] W.J. Ong, L.L. Tan, Y.H. Ng, S.T. Yong, S.P. Chai, Graphitic carbon nitride (g-C_3N_4)-based photocatalysts for artificial photosynthesis and environmental remediation: are we a step closer to achieving sustainability? Chem. Rev. 116 (2016) 7159–7329.

[15] S. Yang, X. Feng, X. Wang, K. Mullen, Graphene-based carbon nitride nanosheets as efficient metal-free electrocatalysts for oxygen reduction reactions, Angew. Chem. Int. Ed. Eng. 50 (2011) 5339–5343.

[16] A.J. Wang, H. Li, H. Huang, Z.S. Qian, J.J. Feng, Fluorescent graphene-like carbon

nitrides: synthesis, properties and applications, J. Mater. Chem. C 4 (2016) 8146–8160.

[17] B. Yuan, Z. Chu, G. Li, T. Hu Z Jiang, Q. Wang, C. Wang, Water-soluble ribbon-like graphitic carbon nitride (g-C_3N_4): green synthesis, self-assembly and unique optical properties, J. Mater. Chem. C 2 (2014) 8212–8215.

[18] H. Zhang, S. Hu Y Huang, Q. Huang, C. Wei, W. Zhang, L. Kang, Z. Huang, A. Hao, Fluorescent probes for “off–on” sensitive and selective detection of mercury ions and L-cysteine based on graphitic carbon nitride nanosheets, J. Mater. Chem. C 3 (2015) 2093–2100.

[19] Z. Teng, H. Lv, L. Wang, L. Liu, C. Wang, G. Wang, Voltammetric sensor modified by EDTA-immobilized graphene-like carbon nitride nanosheets: preparation, characterization and selective determination of ultra-trace Pb(II) in water samples, Electrochim. Acta 212((2016) 722–733.

[20] W. Wei, T. Jacob, Strong excitonic effects in the optical properties of graphitic carbon nitrideg-C_3N_4 from first principles, Phys. Rev. B 87 (2013) 085202.

[21] K.S. Lakhi, D.H. Park, K. Al Bahily, W. Cha, B. Viswanathan, J.H. Choy, A. Vinu, Mesoporous carbon nitrides: synthesis, functionalization, and applications, Chem. Soc. Rev. 46 (2017) 72–101.

[22] P. Niu, L. Zhang, G. Liu, H.M. Cheng, Graphene-like carbon nitride nanosheets for improved photocatalytic activities, Adv. Funct. Mater. 22 (2012) 4763–4770.

[23] K. Sakaushi, M. Antonietti, Carbon- and nitrogen-based organic frameworks, Acc. Chem. Res. 48 (2015) 1591–1600.

[24] J. Zhang, Y. Chen, X. Wang, Two-dimensional covalent carbon nitride nanosheets: synthesis, functionalization, and applications, Energy Environ. Sci. 8 (2015) 3092–3108.

[25] H. Zhao, H. Yu, X. Quan, S. Chen, Y. Zhang, H. Zhao, H. Wang, Fabrication of atomic single layer graphitic-C_3N_4 and its high performance of photocatalytic disinfection under visible light irradiation, Appl. Catal. B Environ. 152-153((2014) 46–50.

[26] L. Zhou, H. Zhang, H. Sun, S. Liu, M.O. Tade, S. Wang, W. Jin, Recent advances in non-metal modification of graphitic carbon nitride for photocatalysis: a historic review, Cat. Sci. Technol. 6 (2016) 7002–7023.

[27] X. Zhang, X. Xie, H. Wang, J. Zhang, B. Pan, Y. Xie, Enhanced photoresponsive ultrathin graphitic-phase C_3N_4 nanosheets for bioimaging, J. Am. Chem. Soc. 135 (2013) 18–21.

[28] Z. Teng, H. Lv, C. Wang, H. Xue, H. Pang, G. Wang, Bandgap engineering of ultrathin graphene-like carbon nitride nanosheets with controllable oxygenous functionalization, Carbon 113((2017) 63–75.

[29] H. Lv, Z. Teng, C. Wang, G. Wang, Ultra-high sensitive voltammetric sensor modified by largely oxygenous functionalized ultrathin carbon nitride nanosheets for detection of Cu(II), Sensors Actuators B Chem. 242((2017) 897–903.

[30] T. Liao, C. Sun, Z. Sun, A. Du, D. Hulicova-Jurcakova, S.C. Smith, How to achieve maximum charge carrier loading on heteroatom-substituted graphene nanoribbon edges: density functional theory study, J. Mater. Chem. 22 (2012) 13751–13755.

[31] X. She, L. Liu, H. Ji, Z. Mo, Y. Li, L. Huang, D. Du, H. Xu, H. Li, Template-free synthesis of 2D porous ultrathin nonmetal-doped g-C_3N_4 nanosheets with highly efficient photocatalytic H_2 evolution from water under visible light, Appl. Catal. B Environ. 187((2016) 144–153.

[32] J. Wu X She, J. Zhong, H. Xu, Y. Yang, R. Vajtai, J. Lou, Y. Liu, D. Du, H. Li, P.M. Ajayan, Oxygenated monolayer carbon nitride for excellent photocatalytic hydrogen evolution and external quantum efficiency, Nano Energy 27((2016) 138–146.

[33] Z. Huang, J. Song, L. Pan, Z. Wang, X. Zhang, J.J. Zou, W. Mi, X. Zhang, L. Wang, Carbon nitride with simultaneous porous network and O-doping for efficient solar-energy-driven hydrogen evolution, Nano Energy 12 (2015) 646–656.

[34] H.J. Li, B.W. Sun, L. Sui, D.J. Qian, M. Chen, Preparation of water-dispersible porous g-C_3N_4 with improved photocatalytic activity by chemical oxidation, Phys. Chem. Chem. Phys. 17 (2015) 3309–3315.

[35] Z.M. Ao, J. Yang, S. Li, Q. Jiang, Enhancement of CO detection in Al doped graphene, Chem. Phys. Lett. 461 (2008) 276–279.

[36] B. Delley, From molecules to solids with the $DMol_3$ approach, J. Chem. Phys. 113 (2000) 7756–7764.

[37] T. Liao, C. Sun, A. Du, Z. Sun, D. Hulicova-Jurcakova, S. Smith, Charge carrier exchange at chemically modified graphene edges: a density functional theory study, J. Mater. Chem. 22 (2012) 8321–8326.

[38] J.P. Perdew, K. Burke, M. Ernzerhof, Generalized gradient approximation made simple, Phys. Rev. Lett. 77 (1996) 3865–3868.

[39] A. Du, S. Sanvito, Z. Li, D. Wang, Y. Jiao, T. Liao, Q. Sun, Y.H. Ng, Z. Zhu, R. Amal, S.C. Smith, Hybrid graphene and graphitic carbon nitride nanocomposite: gap opening, electron-hole puddle, interfacial charge transfer, and enhanced visible light response, J. Am. Chem. Soc. 134 (2012) 4393–4397.

[40] L.X. Ying, Z.J. Min, Formaldehyde molecule adsorbed on doped graphene: a first-principles study, Appl. Surf. Sci. 293((2014) 216–219.

[41] L. Liu, H. Lv, C. Wang, Z. Ao, G. Wang, Fabrication of the protonated graphitic carbon nitride nanosheets as enhanced electrochemical sensing platforms for hydrogen peroxide and paracetamol detection, Electrochim. Acta 206((2016) 259–269.

[42] T. Liao, Z. Sun, C. Sun, S.X. Dou, D.J. Searles, Electronic coupling and catalytic effect on H_2 evolution of MoS_2/graphene nanocatalyst, Sci. Rep. 4 (2014) 6256.